Precision Many-Body Study of the Berezinskii-Kosterlitz-Thouless Transition and Temperature-Dependent Properties in the Two-Dimensional Fermi Gas

Yuan-Yao He,[1,2,3,*] Hao Shi,[4] and Shiwei Zhang[3,†]
[1]*Institute of Modern Physics, Northwest University, Xi'an 710127, China*
[2]*Shaanxi Key Laboratory for Theoretical Physics Frontiers, Xi'an 710127, China*
[3]*Center for Computational Quantum Physics, Flatiron Institute, New York, New York 10010, USA*
[4]*Department of Physics and Astronomy, University of Delaware, Newark, Delaware 19716, USA*

(Received 10 November 2021; revised 13 July 2022; accepted 26 July 2022; published 12 August 2022)

We perform large-scale, numerically exact calculations on the two-dimensional interacting Fermi gas with a contact attraction. Reaching much larger lattice sizes and lower temperatures than previously possible, we determine systematically the finite-temperature phase diagram of the Berezinskii-Kosterlitz-Thouless (BKT) transitions for interaction strengths ranging from BCS to crossover to BEC regimes. The evolutions of the pairing wave functions and the fermion and Cooper pair momentum distributions with temperature are accurately characterized. In the crossover regime, we find that the contact has a nonmonotonic temperature dependence, first increasing as temperature is lowered, and then showing a slight decline below the BKT transition temperature to approach the ground-state value from above.

DOI: 10.1103/PhysRevLett.129.076403

Two-dimensional (2D) correlated fermion systems have been of central interest in condensed matter physics and other areas. They vary from lattice models [1,2] to ultracold quantum gas [3] and real materials [4]. The interplay between the reduced dimensionality and many-body correlation effects in such systems can induce fascinating and unique quantum phenomena, such as Berezinskii-Kosterlitz-Thouless (BKT) phase transitions [5–8] and high-temperature superconductivity [9]. Among them, the 2D Fermi gas with zero-range attractive interaction presents tremendous opportunities as it can be experimentally realized using ultracold atoms [3] in a highly controlled way. The system has already contributed greatly to our understanding of BCS-BEC crossover physics [10–13]. With intense ongoing effort and rapid experimental advances, it is poised to play an even greater role in the quest to understand the physics of 2D correlated fermion systems.

In experiments, the interaction strength of the 2D Fermi gas can be tuned by the scattering length via Feshbach resonance, and a wide range of fermion densities and temperatures can be accessed with great control and precision. Such a dilute Fermi gas system was first realized with a harmonic trap [14–32] and recently in a box potential [33,34]. Early experiments studied the density distribution in a trap [16], the 2D–3D crossover [17,18], polarons [19,20], viscosity [21], the contact parameter [22], pressure [23], followed by the equation of state [27,29]. Superfluidity at low temperatures and the corresponding BKT phase transitions were observed through measurements of the pair condensate [24], first-order correlation function $g_1(r)$ [25] and the critical velocity [34], and the BKT transition temperature in the crossover regime was measured in Ref. [24]. Many more experiments can be expected, with increasing capability, precision, and control. This has stimulated much theoretical and computational activity and opened an avenue for rapid progress through comparison and benchmark.

Theoretically, the 2D Fermi gas is usually described by a model including a simple dispersion (e.g., quadratic) and contact attraction [35]. A variety of approximate theories have been applied, including mean-field analysis [11,36], virial expansion [37,38], and the Luttinger-Ward approach [39–42]. These studies have concentrated on the equation of state, pair correlations, BKT transitions, and the possible pseudogap phenomena. Computationally, ground-state properties have been characterized reasonably well, with fixed-node diffusion Monte Carlo simulations [43,44] and numerically exact auxiliary-field quantum Monte Carlo (AFQMC) method [45,46]. At finite temperatures, a quantum Monte Carlo (QMC) study employing state-of-the-art lattice techniques provided numerically exact results on the pressure, compressibility, and the contact [47]; however, these simulations were still mostly limited to finite lattices of ∼400 sites and in the normal phase at higher temperatures.

In this Letter, we report an *ab initio*, numerically exact study of the finite-temperature properties of the BCS-BEC crossover in the 2D Fermi gas. Implementing recent progress in AFQMC [48], our calculations reach lattice sizes (∼5000 sites) and temperatures ($T_F \sim 0.0125T_F$) far beyond what has been possible with existing methods. This allows us to approach the continuum and thermodynamic limits, and compute quantities previously inaccessible from simulations or determine properties with much higher precision. We obtain the phase diagram of the BKT transition, and characterize the evolution of the pairing wave functions and the fermion and pair momentum distributions. An accurate measure of the contact is provided.

We model the uniform 2D Fermi gas with contact attraction by the following lattice Hamiltonian,

$$\hat{H} = \sum_{\mathbf{k}\sigma} \varepsilon_{\mathbf{k}} c^{+}_{\mathbf{k}\sigma} c_{\mathbf{k}\sigma} + U \sum_{\mathbf{i}} \hat{n}_{\mathbf{i}\uparrow} \hat{n}_{\mathbf{i}\downarrow} - \mu \sum_{\mathbf{i},\sigma} \hat{n}_{\mathbf{i}\sigma}, \quad (1)$$

where σ ($=\uparrow$ or $\downarrow$) denotes spin, and $\hat{n}_{\mathbf{i}\sigma} = c^{+}_{\mathbf{i}\sigma} c_{\mathbf{i}\sigma}$ is the density operator. We have tested both the Hubbard $\varepsilon_{\mathbf{k}} = 4 - 2(\cos k_x + \cos k_y)$ and the quadratic dispersions $\varepsilon_{\mathbf{k}} = k_x^2 + k_y^2$ (corresponding to fermion mass $m = 1/2$ comparing to $\varepsilon_{\mathbf{k}} = \hbar^2 k^2/2m$), where the momentum k_x (and k_y) are defined in units of $2\pi/L$ with the system size $N_s = L^2$. These dispersions, which both have finite effective ranges [49] that vanish as $L \to \infty$, lead to consistent results in the large L limit. The Hubbard dispersion tends to have larger finite-size effects, which are more prominent in the contact. We use it for cross-checks, but all our final results are obtained with the quadratic dispersion. In practical simulations, the chemical potential μ is tuned to reach a fixed number of fermions N_e, resulting in a fermion density $n = N_e/N_s$. The on-site interaction strength U can be determined from $\log(k_F a)$ [45,48,50] (with the Fermi vector $k_F = \sqrt{2\pi n}$ and the 2D scattering length a). We measure temperatures in units of $T_F \equiv E_F/k_B$ (setting $k_B = 1$) with the Fermi energy $E_F = k_F^2 = 2\pi n$. To reach the continuum limit reliably, especially given the delicate nature of the BKT transition, we have simulated lattice sizes up to 75×75. To span the temperature range and make connection with the ground state, we access temperatures as low as $T/T_F = 0.0125$.

Perhaps the most intriguing property of 2D Fermi gas is the BKT phase transition [5,6]. We compute the transition temperatures T_{BKT}/T_F numerically from the condensate fraction in finite systems. The condensate fraction n_c is obtained as the leading eigenvalue of the zero-momentum spin-singlet pairing matrix [45,48]

$$\mathbf{M}_{\mathbf{k}\mathbf{k}'} = \langle \Delta^{+}_{\mathbf{k}} \Delta_{\mathbf{k}'} \rangle - \delta_{\mathbf{k}\mathbf{k}'} \langle c^{+}_{\mathbf{k}\uparrow} c_{\mathbf{k}\uparrow} \rangle \langle c^{+}_{-\mathbf{k}\downarrow} c_{-\mathbf{k}\downarrow} \rangle, \quad (2)$$

divided by $N_e/2$, with $\Delta^{+}_{\mathbf{k}} = c^{+}_{\mathbf{k}\uparrow} c^{+}_{-\mathbf{k}\downarrow}$ as the pairing operator. The corresponding eigenvector gives the pairing wave function in reciprocal space $\phi_{\uparrow\downarrow}(\mathbf{k})$. In a finite-size system the first-order derivative $dn_c/d(T/T_F)$ shows a sharp peak [48], whose location identifies the BKT transition. We fit $n_c(T)$ in each system using a fourth-order polynomial around the transition point, and then compute the peak location of its first-order derivative. We then perform a finite-size extrapolation to obtain T_{BKT} in the thermodynamic limit [51]. (We have also tested using the first-order correlation function and studying its decay exponent, and find the finite-size effects are much larger [52–56].) Systematic errors from finite-size effects are removed or estimated from the extrapolation process [51]. Other systematic errors (Trotter errors, truncation errors) are controlled and smaller than our statistical uncertainties. The latter are estimated from the Monte Carlo process as one standard deviation errors.

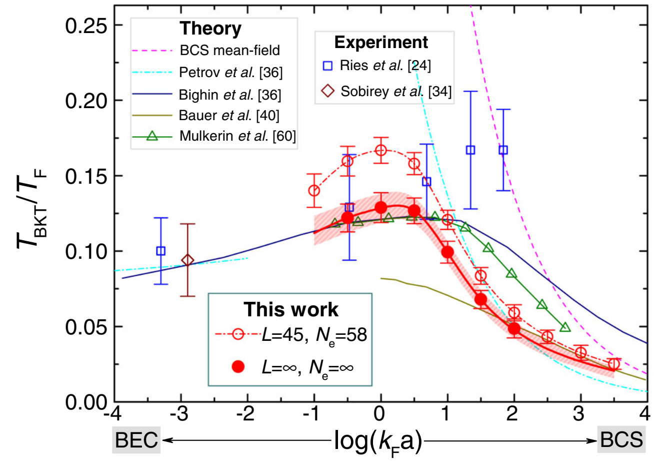

FIG. 1. BKT transition temperatures and phase diagram of the 2D interacting Fermi gas. Empty red circles show our exact results for a finite system of $L = 45$, $N_e = 58$ with quadratic dispersion. Filled red circles show finite-size scaling results to the continuum and thermodynamic limits ($L = \infty$, $N_e = \infty$) for a subset of the interaction strengths. The solid red line connecting these are the results of interpolation, with the shaded band indicating statistical error bars based on both sets of results. For comparison, results are also shown from BCS mean-field theory and its improvement on the BCS side (Petrov *et al.* [36]), the weakly interacting Bose gas on the BEC side (Petrov *et al.* [36]), one-loop Gaussian fluctuation theory (Bighin *et al.* [36]), Luttinger-Ward theory (Bauer *et al.* [40]), Gaussian pair fluctuation theory (Mulkerin *et al.* [60]), and experimental measurements (Ries *et al.* [24] and Sobirey *et al.* [34]).

Our main results are summarized in Fig. 1, which presents the phase diagram of the 2D Fermi gas. The BKT transition temperatures T_{BKT}/T_F are obtained from an extensive set of individual AFQMC calculations, yielding numerically exact solutions for the Hamiltonian $\hat{H}(N_s, N_e)$ on finite lattices. As mentioned, the most accurate finite-temperature results from previous QMC calculations [47] were limited to high temperatures, mostly in the normal phase. Our AFQMC calculations, employing several methodological advances including a low-rank factorization technique, are able to study both normal and superfluid phases by reaching much lower temperatures, and compute properties accurately at the continuum limit by reaching much larger lattice sizes ($N_s \sim 5000$ vs $N_s < 400$). This allows reliable finite-size extrapolation to $N_s \to \infty$ [57–59]. Results of T_{BKT}/T_F are shown for a gas of $L = 45$, $N_e = 58$ for ten interaction strengths spanning the

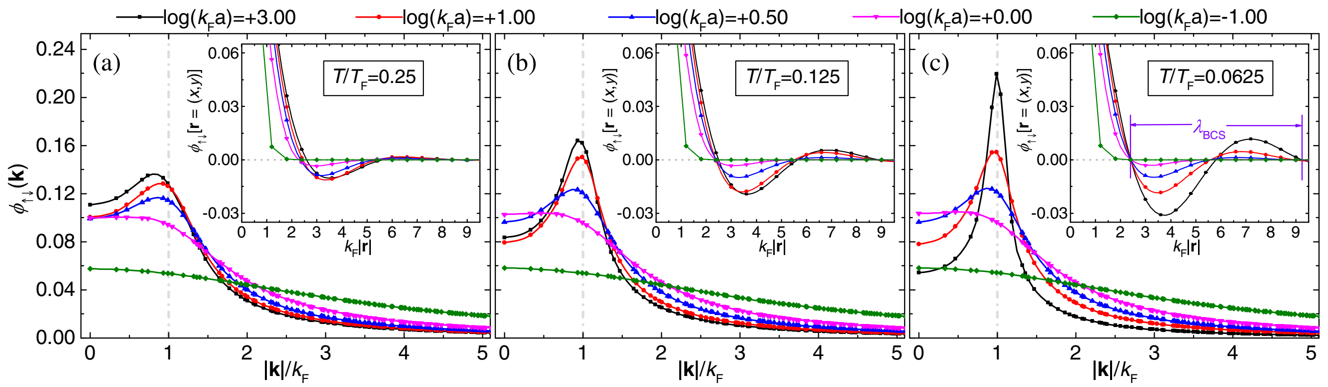

FIG. 2. The singlet pairing wave function in reciprocal space versus $|\mathbf{k}|/k_F$ (main plots), and its Fourier transform, the real space pairing wave function plotted versus $k_F|\mathbf{r}|$ along the diagonal line ($x = y$) (insets). Three temperatures are displayed, from high to low, in the three panels from left to right: (a) $T/T_F = 0.25$, (b) $T/T_F = 0.125$, and (c) $T/T_F = 0.0625$. In each panel five $\log(k_F a)$ values are shown, as indicated by the legends on top, to span the entire range of the interaction strength. The statistical uncertainties are smaller than the symbol size in all cases and are not shown. In the main plots, the Fermi surface is indicated by a vertical dot-dashed line. These calculations are performed with $L = 45$ and $N_e = 58$.

BCS-BEC crossover. Then for selected interaction strengths, we perform systematic finite-size scaling with a range of N_e values (up to 122) [51], each at the continuum limit, to estimate T_{BKT}/T_F at the thermodynamic limit $N_e = \infty$.

The highest BKT transition temperature occurs in the crossover regime, for example at $\log(k_F a) = +0.0$, $T_{\mathrm{BKT}}/T_F = 0.129(9)$ (statistically indistinguishable from the predicted upper bound of 0.125 [61]). This is likely the balance between competing trends. In the weak coupling BCS regime, T_{BKT}/T_F decreases with interaction. On the other hand, as interaction is increased, it is observed that the Cooper pairs become more massive [22], suppressing the tendency for phase coherence. The T_{BKT}/T_F values measured from experiment [24] are also shown in Fig. 1. Experimental error bars are still large but our results are consistent with the measured results in the BEC and crossover regimes. In a more recent experiment [34] the BKT transition temperature is measured in the deep BEC regime [$\log(k_F a) = -2.9$] to be 0.094(24). Although this is well outside the interaction strength we studied, the result seems compatible with the trend in our curve at the smallest $\log(k_F a)$ value. A clear discrepancy is seen in the BCS regime between our results and experiment. This could be due to the experimental analysis procedure [62]. Further investigations are needed which will undoubtedly lead to major progress in this important problem.

In Fig. 2, we show the evolution of the spin-singlet pairing wave function at three temperatures. At low temperature, $T/T_F = 0.0625$ [panel (c)], the system is inside or close to the superfluid phase, and the results are quantitatively close to the ground state values [45], which provide a consistency check. In the BCS regime [$\log(k_F a) = +3.00$], the pairing wave function shows a sharp peak around the Fermi surface, and in real space it extends through the whole system with a wave of approximate wavelength $\lambda_{\mathrm{BCS}} = 2\pi/k_F$, indicating a Cooper pair with size comparable to the system size. In the BEC regime [$\log(k_F a) = -1.00$], the pairing wave function becomes rather flat in reciprocal space, and tightly bound in real space with size much smaller than the interparticle spacing $1/k_F$. Between these limits, the pairing wave function provides a visualization of the crossover process. As the interaction strength increases, the wave function smoothly evolves across a strongly interacting "unitary" regime, with the peak at short distance growing rapidly and the tail of the real-space wave function decaying correspondingly.

Toward higher temperatures $T/T_F = 0.125$ and $T/T_F = 0.25$ as shown in Figs. 2(b) and 2(a), the peak of the pairing wave function $\phi_{\uparrow\downarrow}(\mathbf{k})$ is suppressed. Correspondingly, the tail of the real-space wave function is seen to decay significantly as T/T_F is increased. This trend is more pronounced in the BCS regime at $\log(k_F a) = +3.00$ (black lines). The evolution of the pairing wave function versus temperatures in the crossover and BEC regimes are more gradual. The difference in the pairing wave function appears to be quite mild with respect to whether the system is in the normal or superfluid phase, i.e., whether above or below the transition temperature given in Fig. 1. (A larger difference is seen in the finite-size condensate fraction [51].)

The momentum distributions for fermions and Cooper pairs can be measured in experiments [24]. To allow direct comparisons, we have computed both quantities in our AFQMC calculations. The pair momentum distribution is obtained by extending the pairing matrix in Eq. (2) to Cooper pairs with finite center-of-mass momentum $\mathbf{Q}$ as

$$\mathbf{M}_{\mathbf{k}\mathbf{k}',\mathbf{Q}} = \langle \Delta^{+}_{\mathbf{k}\mathbf{Q}} \Delta_{\mathbf{k}'\mathbf{Q}} \rangle - \delta_{\mathbf{k}\mathbf{k}'} \langle c^{+}_{\mathbf{k}+\mathbf{Q}\uparrow} c_{\mathbf{k}+\mathbf{Q}\uparrow} \rangle \langle c^{+}_{-\mathbf{k}\downarrow} c_{-\mathbf{k}\downarrow} \rangle, \quad (3)$$

with $\Delta^{+}_{\mathbf{k}\mathbf{Q}} = c^{+}_{\mathbf{k}+\mathbf{Q}\uparrow} c^{+}_{-\mathbf{k}\downarrow}$. At each $\mathbf{Q}$, we measure the $\mathbf{M}_{\mathbf{k}\mathbf{k}',\mathbf{Q}}$ matrix, and its leading eigenvalue is identified as the pair momentum distribution $n_{\mathbf{Q}}$. Thus, $n_{\mathbf{Q}=0}$ recovers the condensate fraction result discussed earlier. The

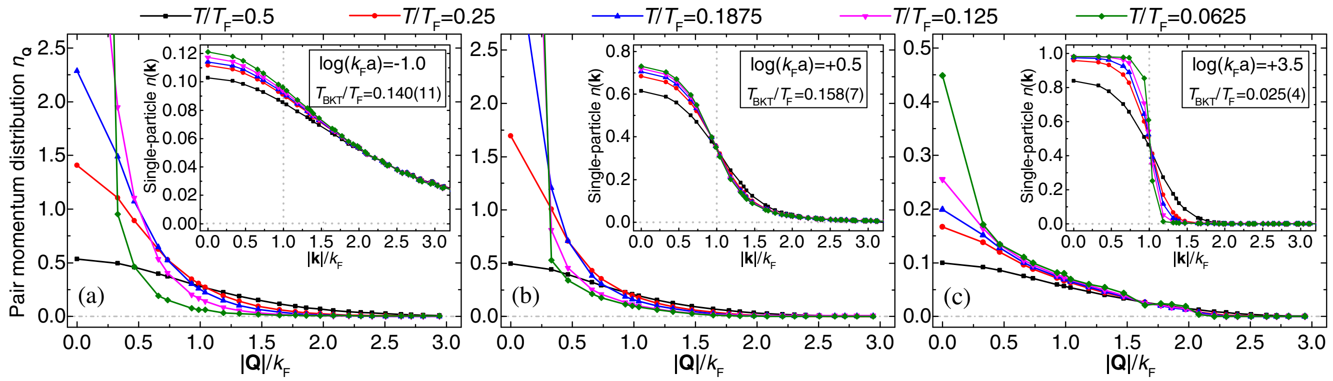

FIG. 3. The momentum distributions for Cooper pairs $n_{\mathbf{Q}}$ versus $|\mathbf{Q}|/k_F$ (main plot) and fermions $n(\mathbf{k})$ versus $|\mathbf{k}|/k_F$ (insets), for three interaction strengths: (a) $\log(k_F a) = -1.0$ in BEC regime, (b) $\log(k_F a) = +0.5$ in crossover regime, and (c) $\log(k_F a) = +3.5$ in BCS regime, with temperatures $T/T_F = 0.0625 \sim 0.5$. These calculations are performed with $L = 45$ and $N_e = 58$, and the corresponding T_{BKT}/T_F values from Fig. 1 are indicated.

results for $n_{\mathbf{Q}}$ are shown in Fig. 3, for three representative interactions. In each case, the pair momentum distribution becomes rapidly centered at $\mathbf{Q} = 0$ as the temperature is decreased. This behavior is consistent with that of a system of interacting bosonic Cooper pairs, in which only the $\mathbf{Q} = 0$ component will survive in the ground state in the bulk limit. At finite temperatures, some of the Cooper pairs can either be broken into individual fermions or simply acquire a velocity (momentum), turning into finite center-of-mass momentum pairs [63]. Furthermore, we find that $\ln n_{\mathbf{Q}}$ exhibits a linear dependence on $(|\mathbf{Q}|/k_F)^2$ [51], consistent with the observation in Ref. [24], which also applied it as a temperature gauge for the experiment. It is particularly interesting to note the behavior of the peak at $\mathbf{Q} = 0$ as T is lowered through T_{BKT}. In the "unitary" regime [panel (b)], the two lowest temperatures are both below T_{BKT}, while the third, $T/T_F = 0.1875$, is above but close to it, as seen in Fig. 1. In comparison, in the BEC regime [panel (a)] only $T/T_F = 0.0625$ is below T_{BKT}, while $T/T_F = 0.125$ is above but close to it. We see that the behavior of the peaks at $\mathbf{Q} = 0$ in these systems shows a direct relation to where they are with respect to the transition temperature.

The fermion momentum distribution is shown for the same systems in the insets of Fig. 3. In contrast with the pair momentum distribution, $n(\mathbf{k})$ shows significantly less temperature dependence. In the weakly interacting BCS regime, we see the steplike function around the Fermi surface at low T, as expected. As T/T_F is increased, more fermions become thermally excited, with $n(\mathbf{k})$ showing substantial modification from the ground-state result at the highest T shown, which is approximately $20 \times T_{\mathrm{BKT}}$. As the interaction strength is increased to the other two values, $n(\mathbf{k})$ is increasingly broader due to interaction effects reflecting the BCS-BEC crossover. However, its response to temperature variation becomes much reduced, and is barely noticeable in the BEC regime. The $n(\mathbf{k})$ results at the lowest temperature is in close agreement with the ground-state results [45].

The contact $\mathcal{C}$ [64–66] is an important quantity in the strongly interacting Fermi gas, and it governs the asymptotic behaviors of several key properties in momentum space, for example, $n(\mathbf{k})$. In the 3D unitary Fermi gas, experimental measurements of the contact across the superfluid transition [67–70] have allowed thorough comparisons with various numerical results [71]. In the 2D Fermi gas, the contact was experimentally measured [22] at $T/T_F = 0.27$ and numerically calculated via ground state QMC methods [43,45]. The contact as a function of temperature was also studied [47], though this was limited to the normal phase and rather small system size as mentioned earlier.

Here, we report exact numerical results of the contact in the full range of temperatures crossing the BKT transition, in large lattice sizes, for the strongly interacting 2D Fermi gas. We compute the contact density $C = \mathcal{C}/N_s$ in units of k_F^4 via the double occupancy D as $C/k_F^4 = m^2U^2D/(4\pi^2 n^2)$. We have also confirmed the asymptotic behavior of $n(\mathbf{k})k^4 \sim \mathcal{C}$ at mediate to low temperatures and extracted the contact by fitting the tail of $n(\mathbf{k})$, which yielded consistent results for $\mathcal{C}$ [51]. Our results of the contact are shown in Fig. 4. While the BCS mean-field theory predicts a phase transition at around $T/T_F \simeq 0.8$ (C_{BCS}/k_F^4 is proportional to the square of the mean-field order parameter), our QMC results show an increase of the C/k_F^4 as the temperature is lowered, followed by a shallow maximum around the BKT transition, and then a decrease which smoothly connects with the ground state result [45]. This behavior is qualitatively different from 3D, where the contact shows a dramatic increase when entering the superfluid phase [69–71].

In summary, employing major advances in AFQMC algorithms, we have studied the finite-temperature properties of 2D Fermi gas with zero-range attractive interaction. Reaching large lattice sizes, we scan a wide range of interaction strengths and temperatures, and determine the phase diagram of the BKT transition. We systematically characterize the BCS-BEC crossover by the pairing wave functions in both reciprocal and real space. We compute

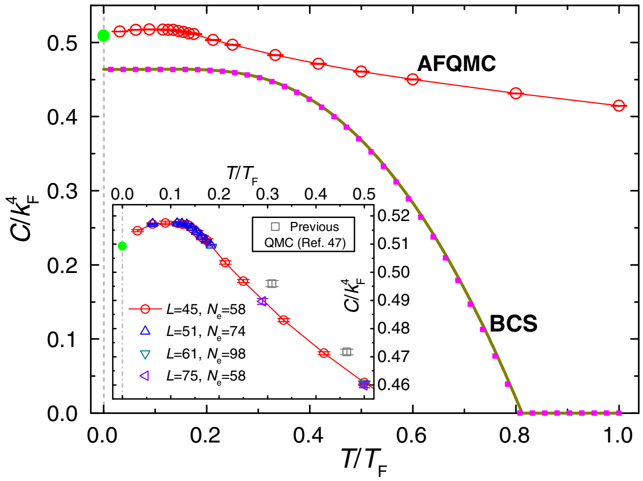

FIG. 4. The contact density C/k_F^4 as a function of temperature in the crossover regime [$\log(k_F a) = +0.50$]. The red open circles represent the $T > 0$ results from our AFQMC calculations. Results at ground state (green solid circle, from Ref. [45]) and from the BCS mean-field theory (dark yellow line for the continuum limit, magenta solid squares for $L = 45$, $N_e = 58$) are also included for comparisons. The inset is an enlargement of the contact density in $T/T_F \in [0, 0.5]$ containing our AFQMC results from different systems up to $L = 75$, and the previous lattice QMC results with $L = 19$ [47].

both the fermion and pair momentum distributions at finite temperatures, and observe behaviors consistent with experimental results. We have also accurately determined the contact versus temperature, and find that it exhibits different behaviors from the 3D case which has been well characterized experimentally.

We hope that these results will serve as a useful guide for experiments, and provide comparison and benchmark for the many analytical and computational studies being stimulated by the intense ongoing experimental efforts. This study also paves the way for further precision many-body computations in the 2D Fermi gas, including effective range effects [72–74], the pseudogap phenomena [15,42,72], and spin-orbit coupling [75], among many others.

We thank Qijin Chen, Xingcan Yao and Wei Zhang for helpful discussions. Y. Y. H. thanks the hospitality of Renmin University of China and Institute of Physics, Chinese Academy of Sciences, where part of this work was done during the academic visits. Y. Y. H. acknowledges the National Natural Science Foundation of China (NSFC) under Grant No. 12047502. The Flatiron Institute is a division of the Simons Foundation.

*heyuanyao@nwu.edu.cn
†szhang@flatironinstitute.org

[1] J. P. F. LeBlanc *et al.* (Simons Collaboration on the Many-Electron Problem), Phys. Rev. X **5**, 041041 (2015).
[2] D. P. Arovas, E. Berg, S. Kivelson, and S. Raghu, Annu. Rev. Condens. Matter Phys. **13**, 239 (2022).
[3] I. Bloch, J. Dalibard, and W. Zwerger, Rev. Mod. Phys. **80**, 885 (2008); S. Giorgini, L. P. Pitaevskii, and S. Stringari, Rev. Mod. Phys. **80**, 1215 (2008).
[4] A. H. Castro Neto, F. Guinea, N. M. R. Peres, K. S. Novoselov, and A. K. Geim, Rev. Mod. Phys. **81**, 109 (2009); V. N. Kotov, B. Uchoa, V. M. Pereira, F. Guinea, and A. H. Castro Neto, Rev. Mod. Phys. **84**, 1067 (2012).
[5] V. L. Berezinsky, Sov. Phys. JETP **34**, 610 (1972), https://inspirehep.net/literature/1716846.
[6] J. M. Kosterlitz and D. J. Thouless, J. Phys. C **6**, 1181 (1973).
[7] J. V. José, *40 Years of Berezinskii-Kosterlitz-Thouless Theory* (World Scientific, Singapore, 2013).
[8] V. N. Ryzhov, E. E. Tareyeva, Y. D. Fomin, and E. N. Tsiok, Phys. Usp. **60**, 857 (2017).
[9] P. A. Lee, N. Nagaosa, and X.-G. Wen, Rev. Mod. Phys. **78**, 17 (2006).
[10] D. M. Eagles, Phys. Rev. **186**, 456 (1969).
[11] P. Nozières and S. Schmitt-Rink, J. Low Temp. Phys. **59**, 195 (1985); M. Randeria, J.-M. Duan, and L.-Y. Shieh, Phys. Rev. Lett. **62**, 981 (1989).
[12] M. Randeria and E. Taylor, Annu. Rev. Condens. Matter Phys. **5**, 209 (2014).
[13] G. C. Strinati, P. Pieri, G. Röpke, P. Schuck, and M. Urban, Phys. Rep. **738**, 1 (2018).
[14] K. Martiyanov, V. Makhalov, and A. Turlapov, Phys. Rev. Lett. **105**, 030404 (2010).
[15] M. Feld, B. Fröhlich, E. Vogt, M. Koschorreck, and M. Köhl, Nature (London) **480**, 75 (2011).
[16] A. A. Orel, P. Dyke, M. Delehaye, C. J. Vale, and H. Hu, New J. Phys. **13**, 113032 (2011).
[17] P. Dyke, E. D. Kuhnle, S. Whitlock, H. Hu, M. Mark, S. Hoinka, M. Lingham, P. Hannaford, and C. J. Vale, Phys. Rev. Lett. **106**, 105304 (2011).
[18] A. T. Sommer, L. W. Cheuk, M. J. H. Ku, W. S. Bakr, and M. W. Zwierlein, Phys. Rev. Lett. **108**, 045302 (2012).
[19] Y. Zhang, W. Ong, I. Arakelyan, and J. E. Thomas, Phys. Rev. Lett. **108**, 235302 (2012).
[20] M. Koschorreck, D. Pertot, E. Vogt, B. Fröhlich, M. Feld, and M. Köhl, Nature (London) **485**, 619 (2012).
[21] E. Vogt, M. Feld, B. Fröhlich, D. Pertot, M. Koschorreck, and M. Köhl, Phys. Rev. Lett. **108**, 070404 (2012).
[22] B. Fröhlich, M. Feld, E. Vogt, M. Koschorreck, M. Köhl, C. Berthod, and T. Giamarchi, Phys. Rev. Lett. **109**, 130403 (2012).
[23] V. Makhalov, K. Martiyanov, and A. Turlapov, Phys. Rev. Lett. **112**, 045301 (2014).
[24] M. G. Ries, A. N. Wenz, G. Zürn, L. Bayha, I. Boettcher, D. Kedar, P. A. Murthy, M. Neidig, T. Lompe, and S. Jochim, Phys. Rev. Lett. **114**, 230401 (2015).
[25] P. A. Murthy, I. Boettcher, L. Bayha, M. Holzmann, D. Kedar, M. Neidig, M. G. Ries, A. N. Wenz, G. Zürn, and S. Jochim, Phys. Rev. Lett. **115**, 010401 (2015).
[26] P. Dyke, K. Fenech, T. Peppler, M. G. Lingham, S. Hoinka, W. Zhang, S.-G. Peng, B. Mulkerin, H. Hu, X.-J. Liu, and C. J. Vale, Phys. Rev. A **93**, 011603(R) (2016).
[27] I. Boettcher, L. Bayha, D. Kedar, P. A. Murthy, M. Neidig, M. G. Ries, A. N. Wenz, G. Zürn, S. Jochim, and T. Enss, Phys. Rev. Lett. **116**, 045303 (2016).

[28] D. Mitra, P. T. Brown, P. Schauß, S. S. Kondov, and W. S. Bakr, Phys. Rev. Lett. **117**, 093601 (2016).
[29] K. Fenech, P. Dyke, T. Peppler, M. G. Lingham, S. Hoinka, H. Hu, and C. J. Vale, Phys. Rev. Lett. **116**, 045302 (2016).
[30] M. Holten, L. Bayha, A. C. Klein, P. A. Murthy, P. M. Preiss, and S. Jochim, Phys. Rev. Lett. **121**, 120401 (2018).
[31] P. A. Murthy, M. Neidig, R. Klemt, L. Bayha, I. Boettcher, T. Enss, M. Holten, G. Zürn, P. M. Preiss, and S. Jochim, Science **359**, 452 (2018).
[32] T. Peppler, P. Dyke, M. Zamorano, I. Herrera, S. Hoinka, and C. J. Vale, Phys. Rev. Lett. **121**, 120402 (2018).
[33] K. Hueck, N. Luick, L. Sobirey, J. Siegl, T. Lompe, and H. Moritz, Phys. Rev. Lett. **120**, 060402 (2018).
[34] L. Sobirey, N. Luick, M. Bohlen, H. Biss, H. Moritz, and T. Lompe, Science **372**, 844 (2021).
[35] A. V. Turlapov and M. Y. Kagan, J. Phys. Condens. Matter **29**, 383004 (2017).
[36] K. Miyake, Prog. Theor. Phys. **69**, 1794 (1983); S. Schmitt-Rink, C. M. Varma, and A. E. Ruckenstein, Phys. Rev. Lett. **63**, 445 (1989); M. Randeria, J.-M. Duan, and L.-Y. Shieh, Phys. Rev. B **41**, 327 (1990); M. Drechsler and W. Zwerger, Ann. Phys. (Berlin) **504**, 15 (1992); D. S. Petrov, M. A. Baranov, and G. V. Shlyapnikov, Phys. Rev. A **67**, 031601(R) (2003); L. Salasnich, Phys. Rev. A **76**, 015601 (2007); W. Zhang, G.-D. Lin, and L.-M. Duan, Phys. Rev. A **77**, 063613 (2008); L. He, H. Lü, G. Cao, H. Hu, and X.-J. Liu, Phys. Rev. A **92**, 023620 (2015); G. Bighin and L. Salasnich, Phys. Rev. B **93**, 014519 (2016).
[37] X.-J. Liu, H. Hu, and P. D. Drummond, Phys. Rev. B **82**, 054524 (2010).
[38] V. Ngampruetikorn, J. Levinsen, and M. M. Parish, Phys. Rev. Lett. **111**, 265301 (2013).
[39] R. Watanabe, S. Tsuchiya, and Y. Ohashi, Phys. Rev. A **88**, 013637 (2013).
[40] M. Bauer, M. M. Parish, and T. Enss, Phys. Rev. Lett. **112**, 135302 (2014).
[41] B. C. Mulkerin, K. Fenech, P. Dyke, C. J. Vale, X.-J. Liu, and H. Hu, Phys. Rev. A **92**, 063636 (2015).
[42] M. Matsumoto, R. Hanai, D. Inotani, and Y. Ohashi, J. Low Temp. Phys. **187**, 668 (2017).
[43] G. Bertaina and S. Giorgini, Phys. Rev. Lett. **106**, 110403 (2011).
[44] A. Galea, H. Dawkins, S. Gandolfi, and A. Gezerlis, Phys. Rev. A **93**, 023602 (2016).
[45] H. Shi, S. Chiesa, and S. Zhang, Phys. Rev. A **92**, 033603 (2015).
[46] E. Vitali, H. Shi, M. Qin, and S. Zhang, Phys. Rev. A **96**, 061601(R) (2017).
[47] E. R. Anderson and J. E. Drut, Phys. Rev. Lett. **115**, 115301 (2015).
[48] Y.-Y. He, H. Shi, and S. Zhang, Phys. Rev. Lett. **123**, 136402 (2019).
[49] J. Carlson, S. Gandolfi, K. E. Schmidt, and S. Zhang, Phys. Rev. A **84**, 061602(R) (2011).
[50] F. Werner and Y. Castin, Phys. Rev. A **86**, 013626 (2012).
[51] See Supplemental Material at http://link.aps.org/supplemental/10.1103/PhysRevLett.129.076403 for further discussions on determination of the BKT transition temperature, momentum distributions, and the contact.
[52] A. Moreo and D. J. Scalapino, Phys. Rev. Lett. **66**, 946 (1991).
[53] R. R. dos Santos, Phys. Rev. B **48**, 3976 (1993).
[54] T. Paiva, R. R. dos Santos, R. T. Scalettar, and P. J. H. Denteneer, Phys. Rev. B **69**, 184501 (2004).
[55] T. Nakano and K. Kuroki, Phys. Rev. B **74**, 174502 (2006).
[56] S. Chandrasekharan and J. C. Osborn, Phys. Rev. B **66**, 045113 (2002).
[57] Y. Tomita and Y. Okabe, Phys. Rev. B **65**, 184405 (2002).
[58] A. Filinov, N. V. Prokof'ev, and M. Bonitz, Phys. Rev. Lett. **105**, 070401 (2010).
[59] P. H. Nguyen and M. Boninsegni, Appl. Sci. **11**, 4931 (2021).
[60] B. C. Mulkerin, L. He, P. Dyke, C. J. Vale, X.-J. Liu, and H. Hu, Phys. Rev. A **96**, 053608 (2017).
[61] T. Hazra, N. Verma, and M. Randeria, Phys. Rev. X **9**, 031049 (2019).
[62] M. Matsumoto, D. Inotani, and Y. Ohashi, Phys. Rev. A **93**, 013619 (2016).
[63] Q. Chen, I. Kosztin, B. Jankó, and K. Levin, Phys. Rev. Lett. **81**, 4708 (1998).
[64] S. Tan, Ann. Phys. (Amsterdam) **323**, 2952 (2008).
[65] S. Tan, Ann. Phys. (Amsterdam) **323**, 2971 (2008).
[66] S. Tan, Ann. Phys. (Amsterdam) **323**, 2987 (2008).
[67] Y. Sagi, T. E. Drake, R. Paudel, and D. S. Jin, Phys. Rev. Lett. **109**, 220402 (2012).
[68] R. J. Wild, P. Makotyn, J. M. Pino, E. A. Cornell, and D. S. Jin, Phys. Rev. Lett. **108**, 145305 (2012).
[69] C. Carcy, S. Hoinka, M. G. Lingham, P. Dyke, C. C. N. Kuhn, H. Hu, and C. J. Vale, Phys. Rev. Lett. **122**, 203401 (2019).
[70] B. Mukherjee, P. B. Patel, Z. Yan, R. J. Fletcher, J. Struck, and M. W. Zwierlein, Phys. Rev. Lett. **122**, 203402 (2019).
[71] S. Jensen, C. N. Gilbreth, and Y. Alhassid, Phys. Rev. Lett. **125**, 043402 (2020).
[72] B. C. Mulkerin, X.-J. Liu, and H. Hu, Phys. Rev. A **102**, 013313 (2020).
[73] H. Hu, B. C. Mulkerin, U. Toniolo, L. He, and X.-J. Liu, Phys. Rev. Lett. **122**, 070401 (2019).
[74] B. C. Mulkerin, H. Hu, and X.-J. Liu, Phys. Rev. A **101**, 013605 (2020).
[75] H. Shi, P. Rosenberg, S. Chiesa, and S. Zhang, Phys. Rev. Lett. **117**, 040401 (2016).